

RESEARCH

Open Access



Glucose deprivation-induced disulfidptosis in human nucleus pulposus cells: a novel pathological mechanism of intervertebral disc degeneration

Shaobo Wu^{1†}, Jin Wang^{2,3†}, Minglin Wang³, Kaisheng Zhou¹, Dageng Huang^{4*}, Yilei Zhang^{3*} and Haihong Zhang^{1*}

Abstract

Background Limited supply of certain nutrients and deregulation of nucleus pulposus (NP) plays a key role in the pathogenesis of intervertebral disc degeneration (IVDD). However, whether nutrient deprivation-induced cell death, particularly disulfidptosis, contributes to the depletion of NP cells and the development of IVDD, is unknown.

Methods RNA-seq, single-cell RNA-seq, and Genome-wide DNA methylation datasets of nucleus pulposus tissue were collected for bioinformatic analysis. Predictive models of disulfidptosis related genes in IVDD were constructed by machine learning and their differential expression was analyzed. In addition, we performed cell subsets identification analysis, cell-cell communications analysis, and functional enrichment analysis of key genes in the core subset based on single-cell RNA-seq data of NP tissues isolated from one normal sample and one IVDD sample. Finally, glucose deprivation-induced disulfidptosis in human NP cells (HNPCs) was verified by various cell death inhibitors and disulfidptosis-related molecular markers.

Results We found the disulfidptosis signal was significantly activated in the IVDD group. Using single-cell RNA-seq analysis, we focused on the chondrocytes and found that disulfidptosis-related genes significantly highly expressed in the IVDD C4 chondrocyte subset, which was identified as a new disulfidptosis-associated cell subset. Correlation analysis revealed the negative correlation between SLC7A11 (driving gene of disulfidptosis) and the glucose transporter GLUTs (SLC2A1-4) family genes (suppressing genes of disulfidptosis) in the IVDD group. We also found obvious cell death in HNPC upon glucose starvation, while employment of various cell death inhibitors could not inhibit glucose starvation-induced death in HNPCs. Moreover, the accumulation of disulfide bonds in cytoskeletal

[†]Shaobo Wu and Jin Wang co-first authors.

*Correspondence:

Dageng Huang
huangdageng@xjtu.edu.cn
Yilei Zhang
zhangyilei@xjtu.edu.cn
Haihong Zhang
ery_zhanghher@lzu.edu.cn

Full list of author information is available at the end of the article



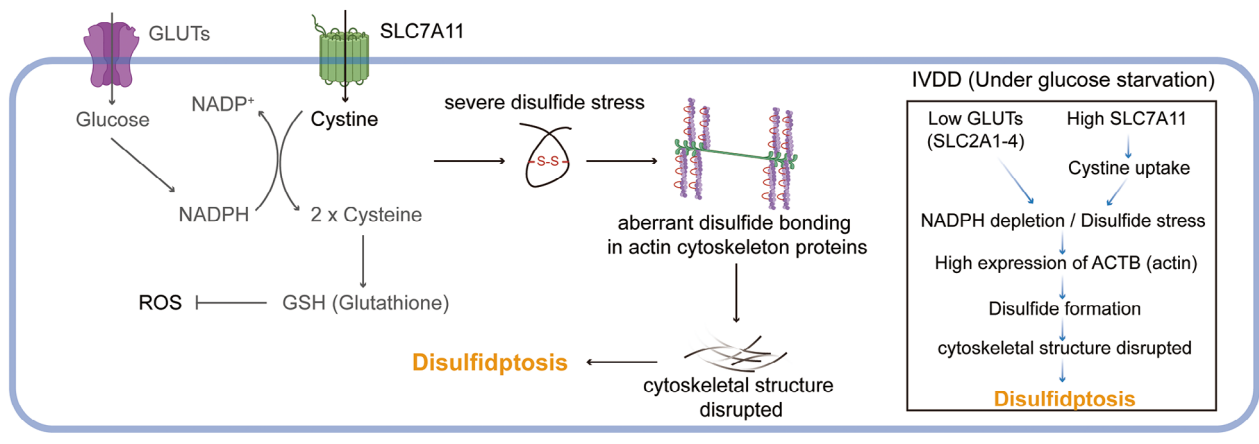
© The Author(s) 2024. **Open Access** This article is licensed under a Creative Commons Attribution-NonCommercial-NoDerivatives 4.0 International License, which permits any non-commercial use, sharing, distribution and reproduction in any medium or format, as long as you give appropriate credit to the original author(s) and the source, provide a link to the Creative Commons licence, and indicate if you modified the licensed material. You do not have permission under this licence to share adapted material derived from this article or parts of it. The images or other third party material in this article are included in the article's Creative Commons licence, unless indicated otherwise in a credit line to the material. If material is not included in the article's Creative Commons licence and your intended use is not permitted by statutory regulation or exceeds the permitted use, you will need to obtain permission directly from the copyright holder. To view a copy of this licence, visit <http://creativecommons.org/licenses/by-nc-nd/4.0/>.

proteins was indicated by slowed migration in non-reducible protein blotting experiments. 2-DG, a key disulfidptosis inhibitor, significantly rescued cell death caused by glucose starvation through lowering the NADP⁺/NADPH ratio.

Conclusions We validated the occurrence of disulfidptosis in HPNCs and identified a novel disulfidptosis-associated cell subset, followed by experimental verification of disulfidptosis in a glucose-limited context to mimic a fall in nutrient supply during the development disc degeneration. These findings provided new insights into the pathological mechanisms of IVDD and encourage us to explore potential therapeutic targets involved in the regulation of disulfidptosis for the prevention of intervertebral disc degeneration.

Keywords Intervertebral disc degeneration, Human nucleus pulposus cells, Disulfidptosis, SLC7A11, NADP⁺/NADPH ratio

Graphical Abstract



Introduction

Low back pain (LBP) is a common problem worldwide, with a prevalence of 22–48%, and intervertebral disc degeneration (IVDD) is one of the most common causes of LBP [1]. Nutrients have been shown to enter the intervertebral discs mainly through the vertebral endplates. With age, degeneration of the endplates prevents nutrients from reaching the intervertebral discs, involved in or accelerates disc degeneration as an initiator of disc degeneration [2]. The center of the disc, where the concentration of nutrients is much lower than in the periphery, is the most sensitive to nutritional changes and is the first to degenerate and die. However, the biological mechanism of nutrient deprivation in IVDD remains unclear and controversial.

Disulfidptosis is a novel form of programmed cell death associated with disulfide stress caused by glucose limitation in cells with high expression of the cystine transporter protein solute carrier family 7 member 11 (SLC7A11; also known as xCT) [3]. SLC7A11-mediated high uptake of cystine results in rapid consumption of NADPH for the reduction of cystine to cysteine. In the context of glucose starvation, pentose phosphate pathway-mediated NADPH generation is blocked. Thus, high SLC7A11-caused NADPH depletion leads to the accumulation of disulfide bonds and subsequent cell death. Specifically, disulfidptosis is currently characterized by

the collapse of cytoskeletal proteins like F-actin, drebrin and MYH9. Therefore, targeting glucose transporters with glucose transporter inhibitor (GLUTi) induces disulfidptosis in cancer cells with high SLC7A11 protein expression, which effectively inhibits tumor growth and provides a new strategy for tumor treatment. However, the presence of disulfidptosis in IVDD and whether it promotes the progression of advanced intervertebral disc degeneration has not yet been reported.

The degenerative process normally begins from the inner part of the disc, known as the nucleus pulposus (NP) [4]. Nucleus pulposus cells (NPCs) are the only constituent cells of the nucleus pulposus of the intervertebral disc, and their abnormal function severely affects the development and progression of IVDD [5]. Bibby's study had found that a significant reduction in cell viability in the absence of glucose, with or without oxygen, suggesting that glucose is a key nutrient in maintaining nucleus pulposus cells viability [6]. However, the presence of newly defined disulfidptosis in IVDD has not been reported, and this is the first study to report the presence and mechanism of disulfidptosis, which contributes to the understanding of the important role of glucose metabolism in intervertebral disc degeneration and provides new strategies for the prevention and treatment of advanced intervertebral disc degeneration.

Methods

Data acquisition and processing

We obtained the gene expression data of nucleus pulposus (NP) tissue of intervertebral disc degeneration (IVDD) patients from the Gene Expression Omnibus (GEO) database (<http://www.ncbi.nlm.nih.gov/geo/>), Using the keyword “Intervertebral Disc Degeneration” and “gene expression” to search for relevant datasets, excluding non-human samples. Pfirrmann grading standards of IVDD was shown in Supplementary Table S1, grade I, II and III are defined as Normal (N) group, grade III and IV are defined as IVDD group. The grouping criteria were derived from the 365 human lumbar disc MRI clinical study by S. Rajasekaran et al. [7]. Including GSE15227 ($N=12$, IVDD=3), GSE23130 ($N=15$, IVDD=8) and GSE70362 ($N=14$, IVDD=10). In addition, Genome-wide DNA methylation expression data was obtained from GSE129789 ($N=8$, IVDD=8), and Single-cell RNA-seq data including one human normal nucleus pulposus tissue and one human degenerative nucleus pulposus tissue was obtained from GSE205535. And, disulfidptosis related genes were derived from Liu's study [3].

Combining machine learning algorithms to create diagnostic model

We applied a total of 15 machine learning algorithms, including: neural network, logistic regression, linear discriminant analysis (LDA), quadratic discriminant analysis (QDA), KNN, decision tree, random forest, XGBoost, ridge regression, Lasso regression, resilient network regression, support vector machine (SVM), gradient boosting machine (GBM), stepwise logistic regression, and simple Bayes. Combinations were performed by caret tuning, custom parameter combination, lasso feature screening and cross-validation, resulting in a total of 207 combined machine learning models. Finally, the model with the highest accuracy was selected by combining the number of samples in the dataset and the associated gene list.

Datasets merge, differential gene analysis and diagnostic ROC

The datasets GSE15227, GSE23130, and GSE70362 were merged into a GEO merged dataset called “Merged Data”. To merge the three GEO datasets, we first merged the datasets using the R package *inSilicoMerging* [8], then removed batch effects using the method of Johnson WE et al. [9] (Empirical Bayes: Adjusting batch effects in microarray expression data using empirical Bayes methods) to remove batch effects, and finally obtained the matrix after removing batch effects, and showed the expression of disulfidptosis related genes in each sample by heat map. In addition, we analyzed the mRNA levels of

disulfidptosis related genes and the corresponding methylation sites by non-parametric tests. ROC analysis was performed on significantly differential expressed genes using the pROC package. The results were visualized by ggplot2 R package.

Functional enrichment analysis of disulfidptosis related genes and protein-protein interaction (PPI) network

The “clusterProfiler” package in R was used to perform Gene ontology (GO) and the Kyoto Encyclopedia of Genes and Genomes (KEGG) [10, 11] enrichment analysis of the disulfidptosis significantly differential expressed genes to clarify the potential pathogenesis and biological pathways. Gene Set Enrichment Analysis (GSEA) is a computational method that determines whether a predefined set of genes has statistically significant, concordant differences between two biological states. In our study, a categorized list of genes was generated based on disulfidptosis genes. This computational approach revealed differences in disulfidptosis related genes between the Normal and IVDD groups. In addition, we used a $p.adjust < 0.05$ to be considered significantly enriched.

STRING (<http://string-db.org>) is an online database widely used for constructing PPI network and scores each interaction between target proteins [12]. We conducted a PPI network analysis of significantly differential expressed genes to explore the interaction under the cut-off of confidence > 0.4 .

Single-cell multi-levels analysis

Nucleus pulposus tissue of degenerating intervertebral discs single cell RNA-seq data was obtained from GSE205535 and analyzed with the “Seurat” package. Degenerated nucleus pulposus tissue samples were obtained from an 81-year-old patient diagnosed with lumbar disc herniation/lumbar disc degeneration, and normal nucleus pulposus tissue samples were obtained from an 11-year-old patient diagnosed with acute spinal cord injury. The sequencing sample information was referred to the study by Li et al. [13]. To retain high-quality data, we eliminated cells with a mitochondrial gene percentage higher than 10%, fewer than three cell counts, fewer than 200 expressed genes, and more than 20,000 genes. For the identification of cell subsets, we selected cell markers by combining previous study [14]. We calculated scores for the disulfidptosis gene set using Seurat's “AddModuleScore” function and analyzed the differences in cell subsets and sample groups. The expression of genes in cell subsets and its ratio in two groups were also analyzed. In addition, we analyzed genes with high and low expression ratio in cell subsets using *irGSEA* (<https://github.com/chuiqin/irGSEA>). This method integrates all single-cell rank-based gene set enrichment analyses and

provides easy visualization of the results. We used different enrichment scoring matrices, including AUCell, UCell, singscore, and ssGSEA aliases. The scoring indicates whether the differential gene set within that cell subset is more or less enriched than the other subsets. And, we evaluated the differential analyses results using the RobustRankAggreg package's robust rank aggregation algorithm (RRA), and filtered out the differential gene set terms that showed a similar degree of enrichment across the four methods.

The CellChat (an algorithm for analyzing intercellular communication at the single-cell level) was used to infer and quantify intercellular communication associated with cell subsets. Information flow was calculated for each signaling pathway, defined as inferring all communication probabilities between all cell pairs in the network.

Cell culture

The immortalized HNPCs (human nucleus pulposus cells) was obtained from IMMOCELL (Xiamen, Fujian, China), and was tested to be mycoplasma contamination-free annually. This cell line was cultured in DMEM supplemented with 10% FBS and 1% penicillin-streptomycin antibiotics in a 5% CO₂ incubator. The glucose-free DMEM was customized from Quanxin Biotechnology (Xi'an, China). Experiments were performed with the glucose-free DMEM (supplemented with 10% dialyzed FBS and 1% penicillin-streptomycin antibiotics). Cells were washed twice with PBS before the experiment to remove as much residual glucose as possible. Then, the experiment was terminated by apparent cell death in the glucose-free condition (about 4 h).

Reagents and antibodies

The cell death inhibitors were purchased as following: Z-VAD-FMK (Sangon Biotech, T7020, Shanghai, China), Necrostatin 2 racemate (Nec-1s, Sangon Biotech, S8641), Liproxstain-1 (Liprox-1, Selleck, S7699, Huston, USA), Chloroquine (CQ, Selleck, S6999). 2-Deoxy-D-glucose (2DG, A602241) was also purchased from Sangon Biotech. The primary antibodies used for Western blotting were as follows: FLNA (A3738), FLNB (A2481) and MYH9 (A0173) were obtained from ABclonal Technology (Wuhan, China). Drebrin (10260-1-AP) and β -Tubulin (66240-1-Ig) were bought from Proteintech (Wuhan, China). SLC7A11 (#12691) were purchased from Cell Signaling Technology (CST, Boston, USA). The concentrations of cell death inhibitors used in this study were as follows: Z-VAD, 5 μ M; Nec-1s, 2 μ M; Liprox-1, 5 μ M; CQ, 20 μ M; 2DG, 10 mM.

Cell viability assays

The CCK8 reagent (K1018, APEX-BIO, Huston, USA) was used to measure cell viability. In brief, cells were seeded

in 96-well plates and treated, then the medium in each well was replaced with 100 μ l of fresh DMEM containing 10% CCK-8 reagent. After 2-hour incubation, the plates were read at an absorbance of 450 nm by a microplate reader (Thermo Scientific, Wilmington, USA).

Western blotting

The reducing and non-reducing western blotting assays were conducted as described in Gan's publication [3]. In brief, cell lysates were harvested in NP-40 buffer. Next, treat the cell lysates with ultrasound and centrifugator, and the supernatants were collected to obtain protein samples. Then, determine the protein concentration and denature the proteins at 95°C for 10 min. Load the same amount of protein on the SDS-PAGE gel, and transfer the separated proteins to a PVDF membrane after electrophoresis. Subsequently, block the membrane in skim milk and followed by incubation of primary and secondary antibodies before visualization.

For non-reducing Western blotting assays, split the protein samples into two aliquots after concentration determination, and mix the aliquots with reducing and non-reducing loading buffer, respectively. Incubate both of the aliquots at 70°C for 10 min for denaturing.

NADP⁺/NADPH measurement

The NADP⁺/NADPH Assay Kit with WST-8 (S0179) was bought from Beyotime Biotechnology (Shanghai, China). This assay was conducted according to the manufacturer's instructions. Briefly, collect the cell lysate with extraction buffer followed by centrifugation. Collect the supernatants and split it into two parts, and heat one part at 60°C for 30 min to remove NADP⁺. Then, transfer both parts of the supernatants to a 96-well plate, then, add G6PDH working solution and chromogenic agent. The formazan amount was measured at 450 nm by a microplate reader.

Statistical analysis

Data acquired from GEO and processed by R programming (4.1.3 version). The Wilcoxon rank-sum test $p < 0.05$ was utilized to determine the statistical significance between groups with different expression levels of genes. The R package "pROC" was used to analyze Receiver-Operating Characteristic (ROC) curve. Correlation analysis was performed with Spearman's correlation test. GO enrichment and KEGG pathway enrichment analyses were conducted using "clusterProfiler" package. The results were all visualized using "ggplot2" R package. Experimental data were presented as mean \pm SEM. GraphPad Prism software was used for statistical graphs and analyses. The comparison between two unpaired groups was performed using Student's t-test. $p < 0.05$ was considered statistically different.

Results

Disulfidptosis related genes mRNA, methylation level differential expression analysis, and machine learning diagnostic models

Multiple machine learning methods were used to predict disulfidptosis related genes diagnostic efficacy of intervertebral disc degenerative disease. The ridge regression 10-fold cross-validation (cutoff=0.25) model had the highest prediction accuracy of 0.701 (Fig. 1A). This highlighted the significance of diagnosing disc degenerative disease through the combined analysis of disulfidptosis related genes. Then, we used heatmap to demonstrate the expression of these genes in the Merged Data samples (Fig. 1B). The results of the differential analysis revealed that 12 genes were significantly highly expressed in the IVDD group: SLC7A11, ACTB, CAPZB, RPN1, DSTN, NDUFS1, NCKAP1, IQGAP1, GCLM, SRXN1, G6PD, and ABCC1 (Fig. 1C). Each of these genes alone had a diagnostic efficacy $AUC > 0.6$ (Fig. 1D). Furthermore, the results of the differential analysis of methylation sites of disulfidptosis related genes showed that the methylation site cg01163369 of the RPN1 gene was significantly overexpressed in the IVDD group (Fig. 1E, F), which is consistent with the significantly high expression of RPN1 mRNA levels. This can be attributed to the fact that cg01163369 is located in the gene body region of the RPN1, which tended to correlate with high gene expression.

Disulfidptosis signal was significantly activated in IVDD

The GSEA analysis showed that disulfidptosis related genes were significantly enriched in the IVDD group ($P_{adj} = 0.01$), indicating that disulfidptosis signal was significantly activated in the IVDD group (Fig. 2A). We constructed a PPI network to identify protein interactions between disulfidptosis related genes (Fig. 2B). Then, we performed functional enrichment analysis on the disulfidptosis related genes and found that the main terms of GO enrichment analysis were actin cytoskeleton, response to oxidative stress, glutathione metabolic process, NADP metabolic process, glucose 6-phosphate metabolic process, NADPH regeneration, and so on (Fig. 2C, D). The main terms of KEGG pathway enrichment were Regulation of actin cytoskeleton, Focal adhesion, Glutathione metabolism, Ferroptosis, Pentose phosphate pathway, and so on (Fig. 2E, F) ($P_{adj} < 0.05$).

Nucleus pulposus cell type annotation and cell communications

Single-cell RNA-seq data was collected from the nucleus pulposus tissue of one normal individual and one patient with disc degeneration (Fig. 3A). Following cell clustering, the nucleus pulposus cells were classified into three types based on the cell markers reported in the previous

study [14]: Chondrocyte, Stromal cell, and Macrophage (Fig. 3B-D). As mature nucleus pulposus cells are a type of chondrocyte, the chondrocyte subset represents the largest percentage of the cells.

From CellChat analysis, the signals communications between overall cell subsets differed somewhat between the normal and IVDD groups (Fig. 4A). In the IVDD group, chondrocyte subset showed reduced signaling to macrophage subset, while signaling to stromal cell subset was enhanced (Fig. 4B). Figure 4C demonstrated specific changes in ligand receptor signaling, with signals for ANNEXIN, CXCL, OSM, VEGF, MPZ, and RANKL being predominantly intense in the IVDD group. Furthermore, we conducted a detailed analysis of the communication signals among the three cell subsets in two groups (Fig. 4D-F). Within the chondrocyte subset, the signal of FN1-CD44 directed towards the stromal cell and macrophage subsets were significantly stronger in the IVDD group compared to the normal group. However, for COL2A1-CD44 signaling, it was significantly stronger in the normal group.

Expression and functional enrichment analysis of disulfidptosis genes

We discovered that disulfidptosis signaling was significantly high expressed in the chondrocyte subset of the IVDD group, among the three cell subsets (Fig. 3E). Furthermore, we used violin plots to demonstrate the expression of disulfidptosis related genes in the three cell subsets, and some genes were also significantly high expressed in the chondrocyte subset (Fig. 3F). We analyzed the chondrocyte expression percentage of several key genes in two groups. The focus was on the chondrocyte. Chondrocytes with high expression of ACTB, CAPZB, SLC7A11 and GCLM had a significantly higher percentage in the IVDD group than normal group (Fig. 3G, H, J, K).

We divided the chondrocytes into two groups based on their expression levels of ACTB and SLC7A11. The functional enrichment analysis showed that chondrocytes with high ACTB expression had significantly higher expression of Unfolded protein response, TNF α signaling via NF- κ B, TGF- β signaling, Apoptosis and Hypoxia, and significantly lower expression of Angiogenesis, and Epithelial mesenchymal transition (Fig. 3I). Chondrocytes with high expression levels of SLC7A11 showed significant upregulation of Unfolded protein response, TNF α signaling via NF- κ B, TGF- β signaling, P53 pathway, Apoptosis, and Hypoxia, and significant downregulation of bile acid metabolism (Fig. 3L).

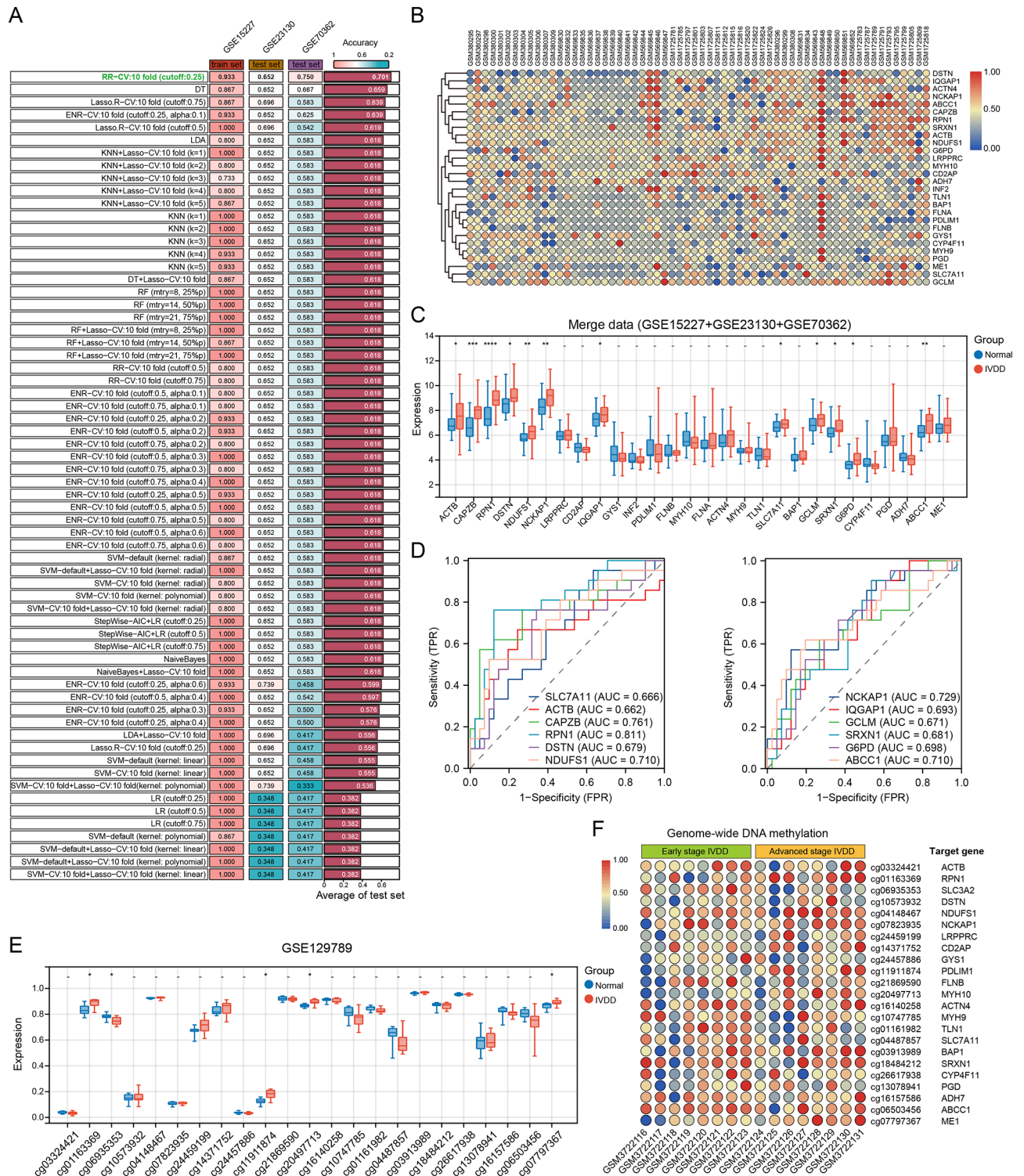


Fig. 1 Construction of predictive models for disulfidptosis related genes and differential expression analysis. **A**. Multiple machine learning approaches to construct disulfidptosis related genes prediction models (in order of model accuracy). **B**. Expression of disulfidptosis related genes in all samples of the Merge data. **C**. Differential expression analysis of disulfidptosis related genes in normal and IVDD groups. **D**. ROC diagnostic model of 12 disulfidptosis related genes with significantly high expression in IVDD group. **E**. Analysis of differences in methylation site levels in the normal and IVDD groups. **F**. Expression of methylation sites corresponding to disulfidptosis genes in the early and advanced stage degeneration groups

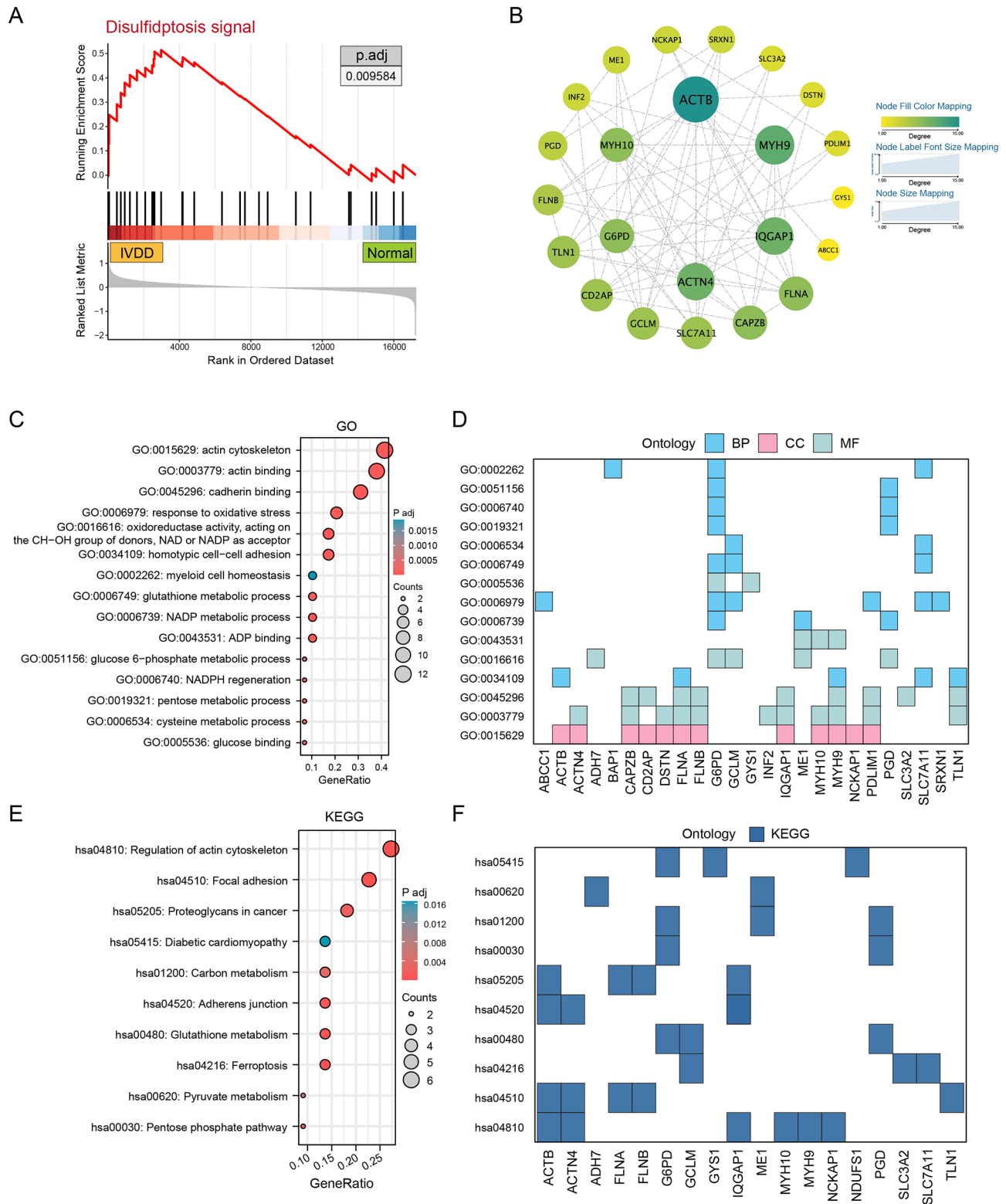


Fig. 2 Disulfidptosis signal was significantly activated in the IVDD group. **A** Enrichment of disulfidptosis signaling in normal and IVDD groups analyzed by GSEA. **B** PPI network of disulfidptosis related proteins. **C** Bubble map for GO enrichment analysis of disulfidptosis related genes. **D** GO enrichment results classification and genes involved in specific terms. **E** Bubble map for KEGG enrichment analysis of disulfidptosis related genes. **F** KEGG enrichment results classification and genes involved in specific terms

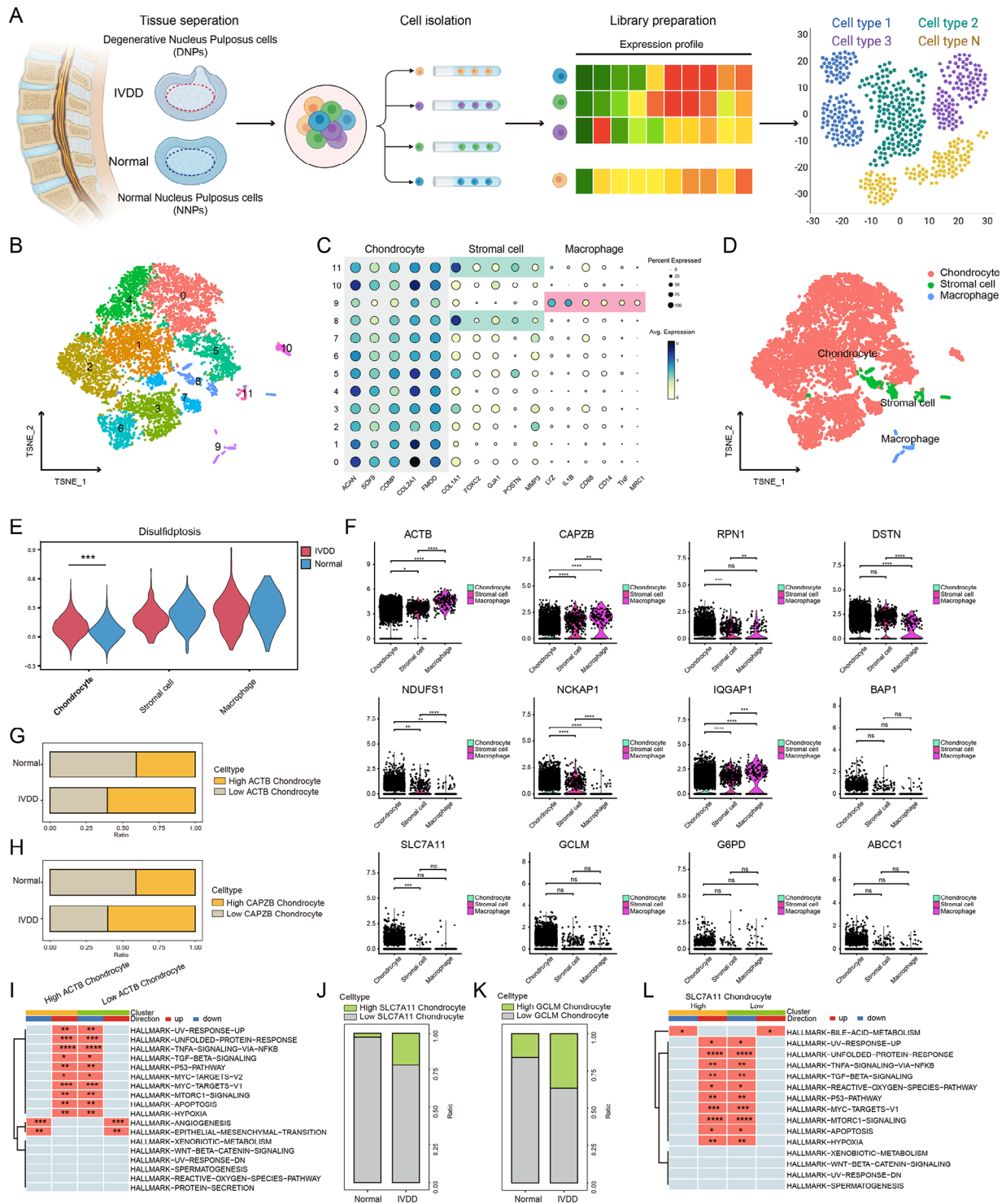


Fig. 3 High expression of disulfidptosis signaling in chondrocyte subset in the IVDD group. **A** Processing of single-cell RNA-seq data from normal and degenerating nucleus pulposus tissues. **B** Original single cell t-Distributed Stochastic Neighbor Embedding (t-SNE) distribution map. **C** Cell markers annotation and cell subsets definition. **D** Three types of cell subsets t-SNE distribution map. **E** Differential expression of disulfidptosis signaling in three cell subsets and two groups. **F** Differential expression of disulfidptosis related genes in cell subsets. **G** Cell proportion with high and low ACTB expression in chondrocytes in normal and IVDD groups. **H** Cell proportion with high and low CAPZB expression in chondrocytes in normal and IVDD groups. **I** Functional enrichment in high and low ACTB expression groups in chondrocytes. **J** Cell proportion with high and low SLC7A11 expression in chondrocytes in normal and IVDD groups. **K** Cell proportion with high and low GCLM expression in chondrocytes in normal and IVDD groups. **L** Functional enrichment in high and low SLC7A11 expression groups in chondrocytes

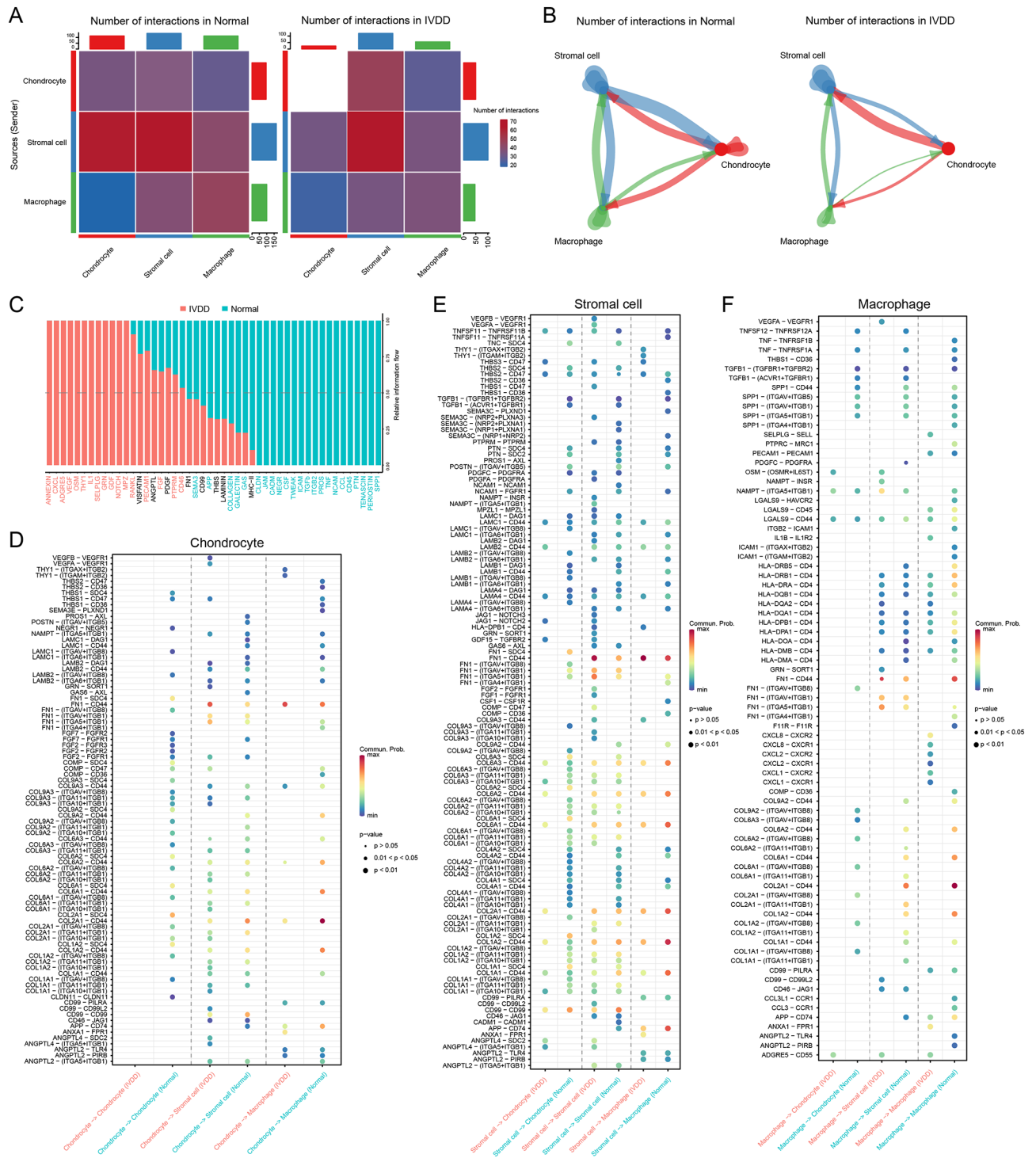


Fig. 4 Cell-cell communications among three cell subsets. **A** Number of interactions in Normal and IVDD groups by heat map. **B** Number of interactions in Normal and IVDD groups by circle diagram. **C** Relative information flow in two groups. **D** Differences in communication signals emitted by chondrocyte between the Normal and IVDD groups. **E** Differences in communication signals emitted by Stromal cell between the Normal and IVDD groups. **F** Differences in communication signals emitted by Macrophage between the Normal and IVDD groups

Identification of disulfidptosis (C4) subset and functional enrichment analysis of specifically expressed genes

Disulfidptosis signal was significantly more highly expressed in the IVDD group among chondrocyte (Fig. 5A). To further investigate chondrocyte subset, we subdivided the chondrocyte subset into five groups: C1-5 cell subsets (Fig. 5B, C). Then, the disulfidptosis

associations were scored for the five subsets by standardized dimensionality reduction clustering and using Seurat’s “AddModuleScore” function. The violin plot illustrated the expression of the disulfidptosis hub genes in C1-5 subsets (Fig. 5E, F). In the IVDD group, we found that the disulfidptosis signal was significantly highly expressed in the C4 subset (Fig. 5D). We defined the C4

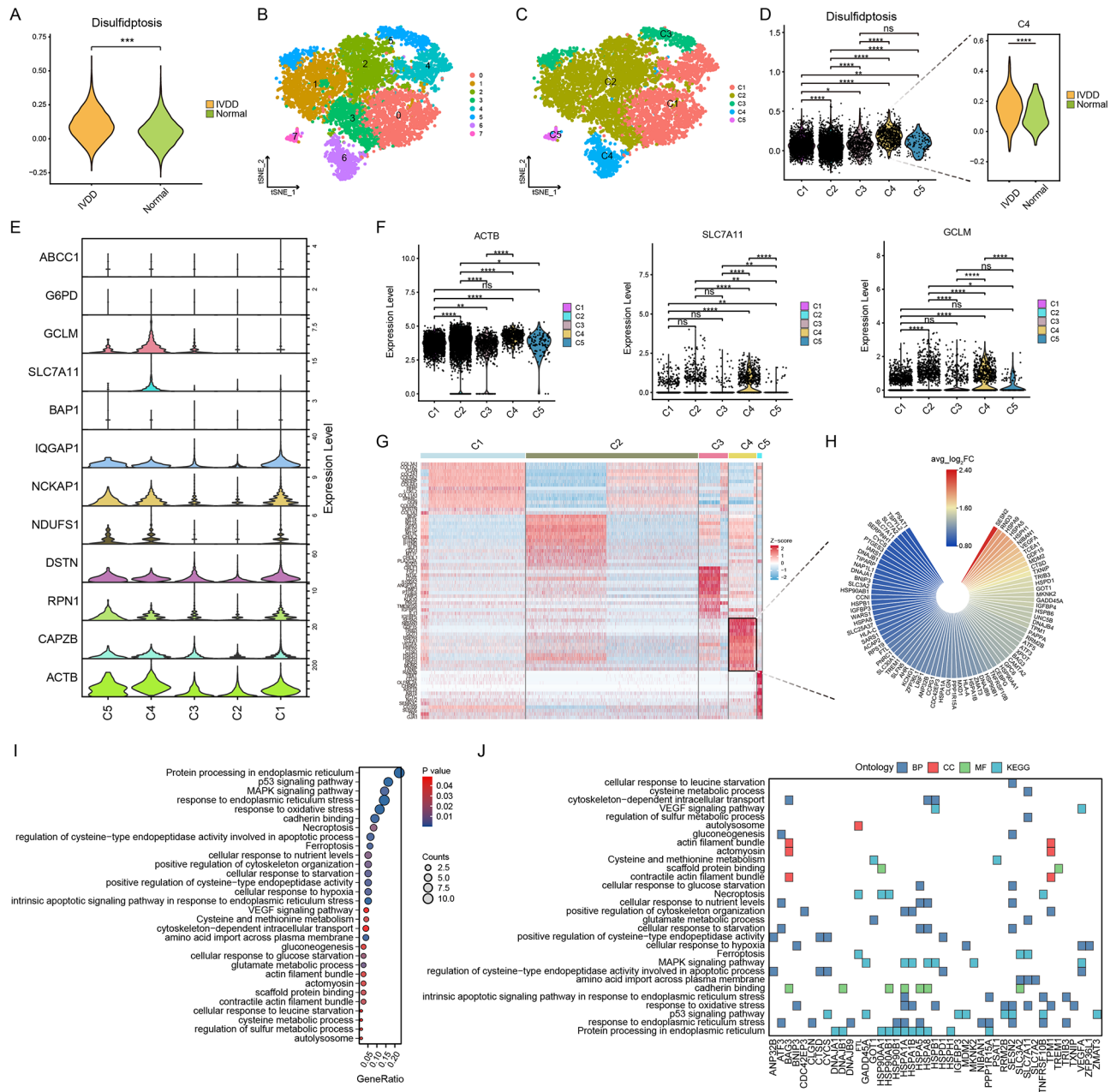


Fig. 5 Chondrocyte C4 cluster identified as the disulfidptosis cell subset. **A** Chondrocyte disulfidptosis signaling is significantly overexpressed in the IVDD group. **B** Original single cell t-Distributed Stochastic Neighbor Embedding (t-SNE) distribution map. **C** C1-C5 cell clusters t-SNE distribution map. **D** Chondrocyte disulfidptosis signaling expression in C1-C5 clusters, significantly overexpressed in the IVDD group C4 cluster. **E** Expression of disulfidptosis hub genes in C1-C5 clusters. **F** Differential expression of ACTB, SLC7A11, and GCLM in C1-C5 clusters. **G** Heatmap showing specifically expressed genes in C1-C5 clusters. **H** Circle plot of fold change of specifically expressed genes in C4 cluster. **I** GO/KEGG enrichment analysis of C4 cluster specifically expressed genes. **J** GO/KEGG enrichment results classification and genes involved in specific terms

as the disulfidptosis cell subset. Then, we performed differential analysis to obtain the set of genes specifically expressed in the C4 and conducted functional enrichment analysis (Fig. 5G, H). The results showed significant enrichment of Protein processing in endoplasmic reticulum, p53, MAPK signaling pathway, response to endoplasmic reticulum stress, response to oxidative stress, Necroptosis, Ferroptosis, cellular response to nutrient levels, Cysteine and methionine metabolism, cellular response to glucose starvation, and so on (Fig. 5I, J).

SLC7A11 negatively correlated with glucose transporters and key enzymes for NADPH production in advanced disc degeneration

To identify potentially relevant nutrient metabolic pathways, we analyzed the correlation between SLC7A11 and 234 SLC family genes (Figure S1) and found that SLC7A11 was associated with the glucose metabolic pathway. The analysis revealed that the glucose transporters SLC2A1-4, were negatively correlated in the IVDD group compared to the normal group (Fig. 6A-D). Specifically, SLC2A1 (GLUT1) showed a significant negative correlation ($p=0.046$, $R = -0.442$). Disulfidptosis may be induced by NADPH depletion. So, we analyzed the correlation between SLC7A11 and six key enzymes that produced NADPH. All of them showed negative correlation compared to the normal group (Figure S2). Furthermore, in the C4 subset, SLC7A11 was significantly positively correlated with cytoskeleton-related genes (Fig. 6E). A schematic diagram illustrated the induction of disulfidptosis by high expression of SLC7A11 combined with low expression of the GLUTs family (Fig. 6F, G).

SLC7A11 was highly expressed under glucose deficiency and induced disulfidptosis in HNPC cells by upregulating the NADP⁺/NADPH ratio

The HNPC cells underwent cell death upon glucose starvation after 4 h treatment (Fig. 7A). To figure out the cell death type in this condition, we used several cell death inhibitors to see if some of them could rescue glucose starvation-induced cell death to some extent (Fig. 7B). However, apoptosis inhibitor Z-VAD, necrosis inhibitor Nec-1s, ferroptosis inhibitor Liprox-1, and autophagic death inhibitor CQ did not save glucose deprivation-induced cell death in HNPC cells, suggesting that this type of cell death is not one of the above. This modality of cell death is very similar to the new cell death mode recently proposed by Gan's group, namely disulfidptosis [3]. Disulfidptosis is tightly regulated by the expression level of SLC7A11. We noted that the expression level of SLC7A11 was up-regulated with prolonged glucose starvation (Fig. 7C). When disulfidptosis occurs, the accumulation of disulfide bonds in cytoskeletal proteins leads to a slower migration following separation under

non-reducing conditions in western blotting assays. As shown in Fig. 7D, under non-reducing conditions, several actin cytoskeleton proteins exhibited significantly slower migration with smears, and some even appeared high-molecular-weight bands close to the stacking layer. Next, we show that 2-Deoxy-D-glucose (2-DG) can rescue cell death upon glucose starvation (Fig. 7E, G). 2-Deoxy-D-glucose is a glucose analog that acts as a competitive inhibitor of glucose metabolism, inhibiting glycolysis via its actions on hexokinase, since its metabolite 2-DG-6-P couldn't be further metabolized in the glycolysis pathway [15]. However, 2-DG-6-P could enter into pentose phosphate pathway and fuel the generation of NADPH, which makes 2DG a good supplement for NADPH production in certain contexts. So, its inhibition of disulfidptosis may be achieved by reducing the NADP⁺/NADPH ratio (Fig. 7F). Together, these results suggest that glucose deprivation can induce disulfidptosis in HNPC cells, possibly through up-regulation of NADP⁺/NADPH ratio.

Discussions

Intervertebral disc degeneration (IVDD) is a global health problem and a major cause of low back pain (LBP) [16], characterized by a homeostatic imbalance between anabolic and catabolic metabolism leading to extracellular matrix (ECM) degradation and nucleus pulposus (NP) cell death [17]. In our study, we firstly defined a unique disulfidptosis cell subset in the nucleus pulposus cells and found that disulfidptosis occurred in human NP cells induced by up-regulation of NADP⁺/NADPH under glucose deficiency.

Firstly, we found that significant cell death occurred in human nucleus pulposus cells after 4 h of glucose deprivation. In advanced disc degeneration, one study used finite elements to analyze changes in metabolites within the disc after endplate calcification: oxygen and glucose concentrations were reduced by 69.3% and 33.9% respectively. Cell viability was significantly reduced in the absence of glucose, with or without oxygen [6]. Liu et al. [3] found that glucose deficiency leads to the death of tumor cells with high SLC7A11 expression, called Disulfidptosis, a new cell programmed death. This cell death was found to result from excessive intracellular disulfide pressure under glucose-deficient conditions, which can be used as a new nutritional therapeutic strategy. However, it has not been reported and studied in IVDD.

We are the first to reveal the mechanism of disulfidptosis in nucleus pulposus cells of the intervertebral disc. We evaluated the expression and diagnostic efficacy of disulfidptosis-related genes in IVDD. By using RNA-seq combined with three datasets, we found that 12 disulfidptosis related genes were significantly highly expressed in the IVDD group, and the accuracy of disease prediction models constructed by machine learning was more

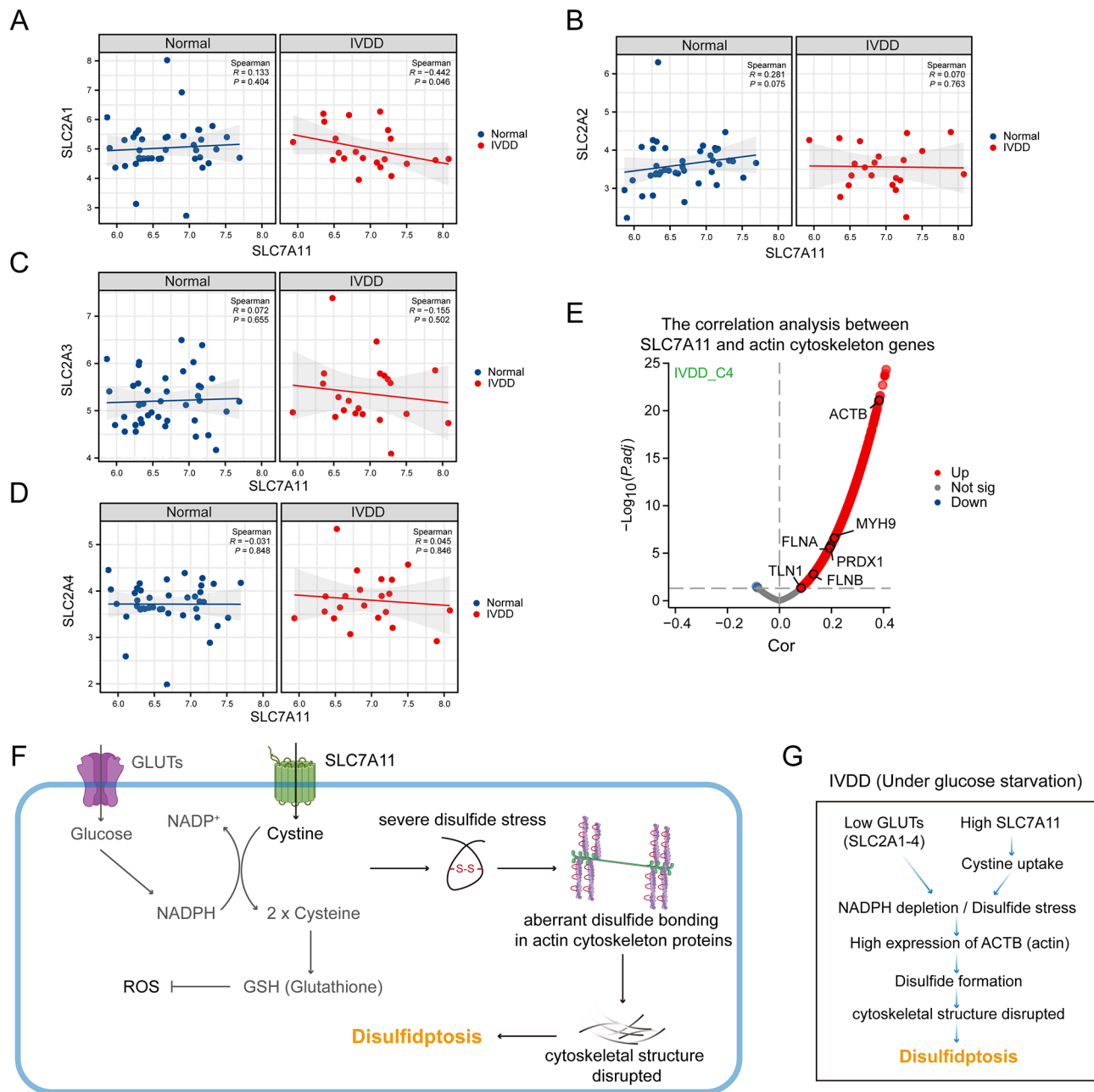


Fig. 6 High expression of SLC7A11 combined with low expression of GLUTs in IVDD group. **A** Correlation analysis between SLC7A11 and SLC2A1 (GLUT1) in normal and IVDD groups. **B** Correlation analysis between SLC7A11 and SLC2A2 (GLUT2) in normal and IVDD groups. **C** Correlation analysis between SLC7A11 and SLC2A3 (GLUT3) in normal and IVDD groups. **D** Correlation analysis between SLC7A11 and SLC2A4 (GLUT4) in normal and IVDD groups. **E** Correlation analysis between SLC7A11 and cytoskeleton-related genes in IVDD C4 cluster. **F, G.** Schematic diagrams illustrated the mechanism of disulfidptosis in IVDD

than 0.7. Combined with Genome-wide DNA methylation expression data, we found that the high expression of RPN1 in IVDD may be due to the increased methylation level of the cg01163369 locus located in the gene body. Gene body methylation level positively correlates with gene expression level [18]. It has been found that RPN1 may be a new diagnostic biomarker for OP patients and

may serve as a new target for kaempferol to improve OP [19].

There are few experimental studies of disulfidptosis in the bone research field. One study found that nuclear factor of activated T-cells 1 (NFATc1) up-regulates the expression of SLC7A11 during RANKL-induced osteoclast genesis, which leads to increased cell disulfide bond stress and disulfidptosis, so selective killing of osteoclast

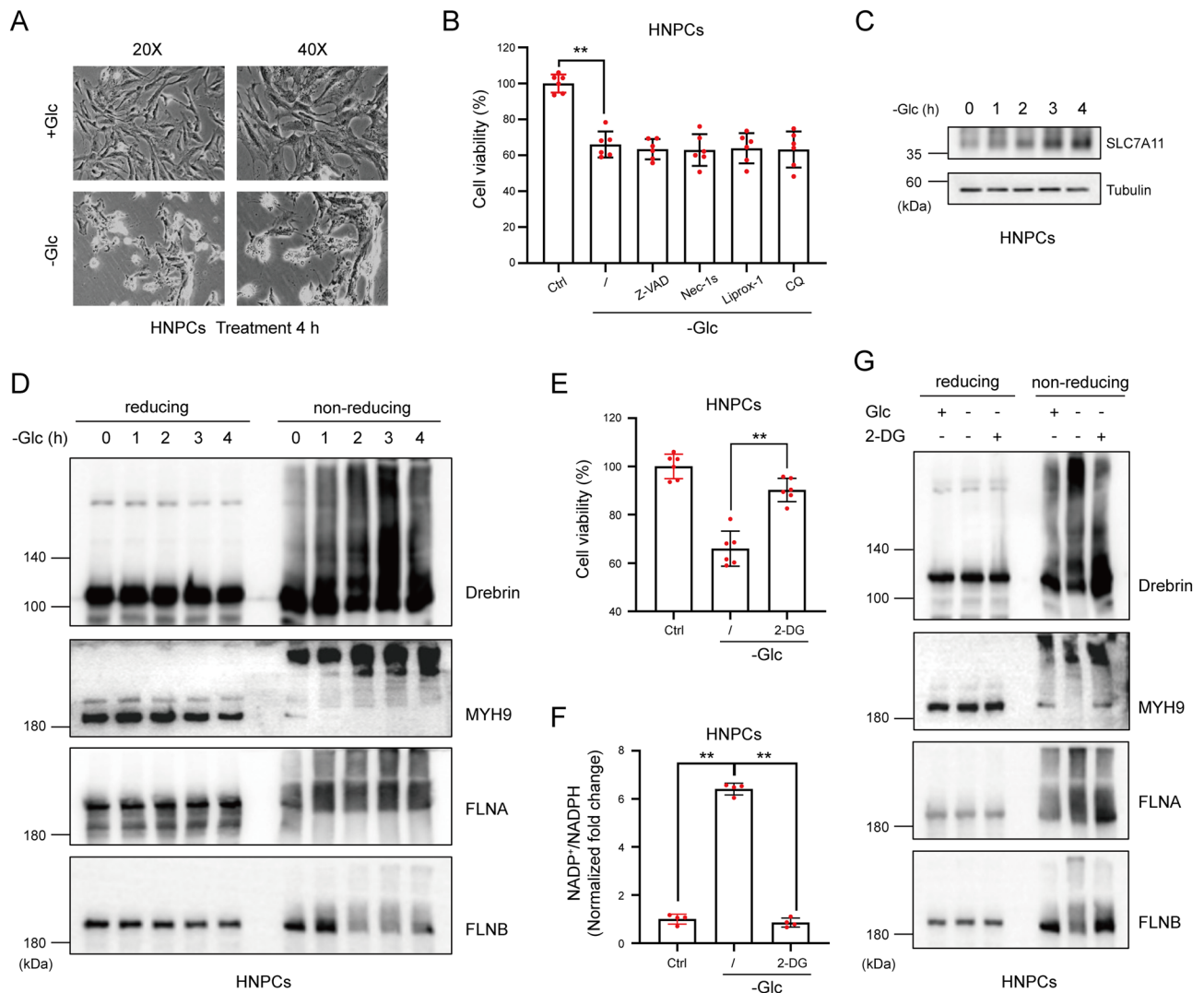


Fig. 7 Glucose starvation induced disulfidptosis in HNPC cells. **A.** HNPC cells died after glucose deprivation for 4 h. **B.** Known cell death inhibitors Z-VAD, Nec-1s, Liprox-1 and CQ cannot rescue cell death induced by glucose deprivation. **C.** Alterations in SLC7A11 expression levels upon glucose starvation. **D.** Reducing and non-reducing Western blotting analysis of actin cytoskeleton proteins in HNPC cells upon glucose deprivation. **E.** 2-DG saved glucose starvation-induced disulfidptosis in HNPC cells. **F.** NADP⁺/NADPH ratio was upregulated upon glucose starvation, and was rescued by 2-DG treatment. **G.** 2-DG alleviated the disulfide stress in HNPC cells upon glucose starvation

precursors using a TXNRD1 inhibitor could provide a potential target for clinical therapy [20]. We also found that this cell death occurred under glucose starvation was not one of the known cell deaths, as four cell death inhibitors were unable to rescue the death of HNPCs under glucose starvation. But, most importantly, we found that the accumulation of disulfide bonds in cytoskeletal proteins leads to a slowing of migration when disulfidptosis occurred by non-reducing protein blotting experiments, which was the key experiment that was missing in the OP study [20]. Thus, by combining the two conditions, we have shown that HNPCs cell death under glucose-deficient conditions is disulfidptosis. Our study also provided new insights for the prevention and treatment of intervertebral disc degeneration.

In Gan et al.'s study, they found that high expression of SLC7A11 leads to depletion of the intracellular NADPH pool, which results in a breakdown of redox homeostasis, excessive accumulation of disulfide bonds and disulfidptosis occurred [3]. They demonstrated in their paper that 2DG treatment provides NADPH through the pentose phosphate pathway and that disulfidptosis is caused by NADPH depletion. Similarly, we found that 2-DG rescued cell death during glucose starvation and inhibited disulfidptosis by reducing the NADP⁺/NADPH ratio. Abnormal disulfide bonds in actin cytoskeleton proteins and F-actin collapse in a SLC7A11-dependent manner [3]. In the disulfidptosis cell subset C4, we similarly found a significant positive correlation between SLC7A11 and related proteins. SLC7A11 high tumor cells can take

up cystine in excess, which is rapidly reduced to cysteine by NADPH, leading to NADPH depletion. SLC7A11 was negatively correlated with the glucose transporters (GLUTs, SLC2A1-4) family genes in the IVDD group. We also noted that the expression level of SLC7A11 was up-regulated with prolonged glucose starvation in HNPCs. Thus, SLC7A11 may serve as a novel target to prevent HNPCs from undergoing disulfidptosis. In addition to the NADPH mechanism, we identified a novel subset of chondrocytes, defined as the disulfidptosis cell subset, by single-cell RNA-seq analysis. Functional enrichment analysis of disulfidptosis cell subset genes revealed significant activation of endoplasmic reticulum (ER) stress. We also performed functional enrichment of chondrocytes in the high and low SLC7A11 expression groups, which also revealed significant activation of the unfolded protein response pathway in the high expression group. Thus, SLC7A11 may be involved in the disulfidptosis occurred through activation of the ER stress pathway.

In conclusion, our study also has limitations, although to the best of our knowledge, this is the first study of disulfidptosis in the field of disc degeneration. However, due to the specificity of the patients, we need more samples for follow-up studies. Secondly, although we have demonstrated the existence of disulfidptosis in human nucleus pulposus cells, the underlying signaling pathways and the role of targeting disulfidptosis in IVDD need to be further elucidated. Our discovery of new cellular subpopulations and the disulfide death phenotype may open a new window for the prevention and treatment of IVDD.

Supplementary Information

The online version contains supplementary material available at <https://doi.org/10.1186/s13062-024-00528-4>.

Supplementary Material 1

Supplementary Material 2: Figure S1. Correlation analysis between SLC7A11 and 234 SLC family genes.

Supplementary Material 3: Figure S2. Correlation analysis between SLC7A11 and six key enzymes that produced NADPH. A. Correlation analysis between SLC7A11 and PGD in normal and IVDD groups. B. Correlation analysis between SLC7A11 and ALDH1L1 in normal and IVDD groups. C. Correlation analysis between SLC7A11 and MTHFD1 in normal and IVDD groups. D. Correlation analysis between SLC7A11 and IDH1 in normal and IVDD groups. E. Correlation analysis between SLC7A11 and ME1 in normal and IVDD groups. F. Correlation analysis between SLC7A11 and G6PD in normal and IVDD groups.

Acknowledgements

Not applicable.

Author contributions

Shaobo Wu and Jin Wang were major contributors in methodology, investigation, and writing. Minglin Wang, Kaisheng Zhou were responsible for the formal analysis and data curation. Dageng Huang, Yilei Zhang, and Haihong Zhang were responsible for the conceptualization and production of this study. All authors wrote the original draft and approved the final manuscript.

Funding

The authors are grateful for the funding supports from National Natural Science Foundation of China (grant no.31960175 to H. Zhang, and 82372847 to Y. Zhang), Natural Science Foundation of Gansu Province (23JRRA0960 to H. Zhang) and the Special Support Project for High-level Talents of Shaanxi Province (2020 to D Huang).

Data availability

No datasets were generated during the current study, the specific analysis of datasets was in the Methods section.

Declarations

Ethics approval and consent to participate

Not applicable.

Consent for publication

Not applicable.

Competing interests

The authors declare no competing interests.

Author details

¹Department of Orthopaedics, Lanzhou University Second Hospital, Lanzhou, Gansu 730030, China

²The Key Laboratory of Tumor Molecular Diagnosis and Individualized Medicine of Zhejiang Province, Zhejiang Provincial People's Hospital, Affiliated People's Hospital, Hangzhou Medical College, Hangzhou, Zhejiang 311300, China

³The Institute of Molecular and Translational Medicine, Department of Biochemistry and Molecular Biology, School of Basic Medical Sciences, Xi'an Jiaotong University Health Science Center, Xi'an, Shaanxi 710061, China

⁴Department of Spine Surgery, Honghui Hospital, Xi'an Jiaotong University, Xi'an, Shaanxi 710054, China

Received: 10 July 2024 / Accepted: 4 September 2024

Published online: 12 September 2024

References

1. Yeh BY, Liu GH, Lee TY, Wong AM, Chang HH, Chen YS. Efficacy of electronic acupuncture shoes for chronic low back Pain: double-blinded Randomized Controlled Trial. *J Med Internet Res*. 2020;22:e22324.
2. Li H, Yan JZ, Chen YJ, Kang WB, Huang JX. Non-invasive quantification of age-related changes in the vertebral endplate in rats using in vivo DCE-MRI. *J Orthop Surg Res*. 2017;12:169.
3. Liu X, Nie L, Zhang Y, Yan Y, Wang C, Colic M, Olszewski K, Horbath A, Chen X, Lei G, Mao C, Wu S, Zhuang L, Poyurovsky MV, James You M, Hart T, Billadeau DD, Chen J, Gan B. Actin cytoskeleton vulnerability to disulfide stress mediates disulfidptosis. *Nat Cell Biol*. 2023;25:404–14.
4. Feng G, Zhang Z, Dang M, Zhang X, Doleyres Y, Song Y, Chen D, Ma PX. Injectable nanofibrous spongy microspheres for NR4A1 plasmid DNA transfection to reverse fibrotic degeneration and support disc regeneration. *Biomaterials*. 2017;131:86–97.
5. Tang N, Dong Y, Chen C, Zhao H. Anisodamine Maintains the Stability of Intervertebral Disc Tissue by inhibiting the senescence of Nucleus Pulposus cells and degradation of Extracellular Matrix via Interleukin-6/Janus Kinases/Signal Transducer and activator of transcription 3 pathway. *Front Pharmacol*. 2020;11:519172.
6. Bibby SR, Urban JP. Effect of nutrient deprivation on the viability of intervertebral disc cells. *Eur Spine J*. 2004;13:695–701.
7. Rajasekaran S, Venkatadass K, Naresh Babu J, Ganesh K, Shetty AP. Pharmacological enhancement of disc diffusion and differentiation of healthy, ageing and degenerated discs: results from in-vivo serial post-contrast MRI studies in 365 human lumbar discs. *Eur Spine J*. 2008;17:626–43.
8. Taminiau J, Meganck S, Lazar C, Steenhoff D, Coletta A, Molter C, Duque R, Schaezen Vd, Weiss DY, Solís H, Bersini, Nowé A. Unlocking the potential of publicly available microarray data using inSilicoDb and inSilicoMerging R/Bioconductor packages. *BMC Bioinformatics*. 2012;13:335.

9. Johnson WE, Li C, Rabinovic A. Adjusting batch effects in microarray expression data using empirical Bayes methods. *Biostatistics*. 2007;8:118–27.
10. Kanehisa M, Furumichi M, Sato Y, Kawashima M, Ishiguro-Watanabe M. KEGG for taxonomy-based analysis of pathways and genomes. *Nucleic Acids Res*. 2023;51:D587–92.
11. Kanehisa M, Goto S. KEGG: kyoto encyclopedia of genes and genomes. *Nucleic Acids Res*. 2000;28:27–30.
12. Szklarczyk D, Kirsch R, Koutrouli M, Nastou K, Mehryary F, Hachilif R, Gable AL, Fang T, Doncheva NT, Pyysalo S, Bork P, Jensen LJ, von Mering C. The STRING database in 2023: protein-protein association networks and functional enrichment analyses for any sequenced genome of interest. *Nucleic Acids Res*. 2023;51:D638–46.
13. Li Z, Ye D, Dai L, Xu Y, Wu H, Luo W, Liu Y, Yao X, Wang P, Miao H, Xu J, Liang W. Single-cell RNA sequencing reveals the difference in human normal and degenerative nucleus Pulposus tissue profiles and Cellular interactions. *Front Cell Dev Biol*. 2022;10:910626.
14. Zhang Y, Han S, Kong M, Tu Q, Zhang L, Ma X. Single-cell RNA-seq analysis identifies unique chondrocyte subsets and reveals involvement of ferroptosis in human intervertebral disc degeneration. *Osteoarthritis Cartilage*. 2021;29:1324–34.
15. Zhu Z, Jiang W, McGinley JN, Thompson HJ. 2-Deoxyglucose as an energy restriction mimetic agent: effects on mammary carcinogenesis and on mammary tumor cell growth in vitro. *Cancer Res*. 2005;65:7023–30.
16. Peng X, Zhang C, Bao JP, Zhu L, Shi R, Xie ZY, Wang F, Wang K, Wu XT. A20 of nucleus pulposus cells plays a self-protection role via the nuclear factor-kappa B pathway in the inflammatory microenvironment. *Bone Joint Res*. 2020;9:225–35.
17. Ni W, Zhang F, Zheng L, Wang L, Liang Y, Ding Y, Yik JHN, Haudenschild DR, Fan S, Hu Z. Cyclin-dependent kinase 9 (CDK9) inhibitor atavociclib suppresses intervertebral Disk Degeneration via the inhibition of the NF- κ B signaling pathway. *Front Cell Dev Biol*. 2020;8:579658.
18. To TK, Saze H, Kakutani T. DNA methylation within transcribed regions. *Plant Physiol*. 2015;168:1219–25.
19. Pan C, Zhang C, Lin Z, Liang Z, Cui Y, Shang Z, Wei Y, Chen F. Disulfidptosis-related protein RPN1 may be a novel anti-osteoporosis target of Kaempferol. *Comb Chem High Throughput Screen* (2024).
20. Zhong Z, Zhang C, Ni S, Ma M, Zhang X, Sang W, Lv T, Qian Z, Yi C, Yu B. NFATc1-mediated expression of SLC7A11 drives sensitivity to TXNDR1 inhibitors in osteoclast precursors. *Redox Biol*. 2023;63:102711.

Publisher's note

Springer Nature remains neutral with regard to jurisdictional claims in published maps and institutional affiliations.